

Comparison of Pulse-shape Discrimination (PSD) Performance Using the Pixelated Stilbene and Plastic Scintillator (EJ-276) Arrays for the Hand-held Dual-particle Imager

Jihwan Boo, Seoryeong Park, and Manhee Jeong*

Department of Nuclear and Energy Engineering, Jeju National University, Jeju 63243, Republic of Korea

*Corresponding author: mhjeong@jejunu.ac.kr

1. Introduction

Special nuclear material (SNM) (plutonium, or uranium enriched to higher than 20% ^{235}U) can have weapons applications. Because SNM has its key characteristics (the energy of emitted neutron and gamma-ray radiation), a combination of the photon and neutron imaging systems called dual-particle imager (DPI) is particularly appealing to nuclear safeguarding applications [1]. DPI that mainly use the neutron-scatter method have been developed [2-4] using the technique, called as pulse-shape discrimination (PSD) [5], discriminating the gamma-ray and the neutron, and create radiation images for both localization and identification.

There has been attempt to use a pixelated detector for the suitability of hand-held DPI application [6]. It was, to the authors knowledge, first time to carry out pulse shape discrimination (PSD) performance test using pixelated arrangement type that has 13×13 square array and a small pixel size ($2.8 \times 2.8 \times 15 \text{ mm}^3$) of plastic scintillator (EJ-299-34). It was reported that there was a fatal degradation of PSD performance in the pixelated crystal array when compared to a single crystal. The PSD performance of the pixelated array, however, could not yet be fully verified because they detected ^{252}Cf stored in a water tank that reduced the average energy (2.1–2.5 MeV) of the fast neutron by one-third (0.7-0.9MeV). Furthermore, because the estimation of PSD performance was performed across the entire energy spectrum, the results were biased toward the low energy events that generally represent the highest misclassification probability in most organic scintillators [7]. They were also not capable of show pixel-by-pixel PSD performance because the pixelated array was mounted on a single-channel photomultiplier tube (PMT) rather than pixelated photodetectors, such as silicon photomultiplier (SiPM).

At the previous KNS spring meeting, we presented the performance of dual-particle imagers using stilbene array (Inrad Optics) coupled with silicon photomultipliers (SiPMs, ArrayC-30035-144P, On Semiconductor) array. In this paper, we will present the comparison of PSD performance on both pixelated stilbene and plastic array (EJ-276, formerly EJ-299-33A, Eljen Technology) when varying internal and outer gain in the dual-particle imager.

2. Methods and Results

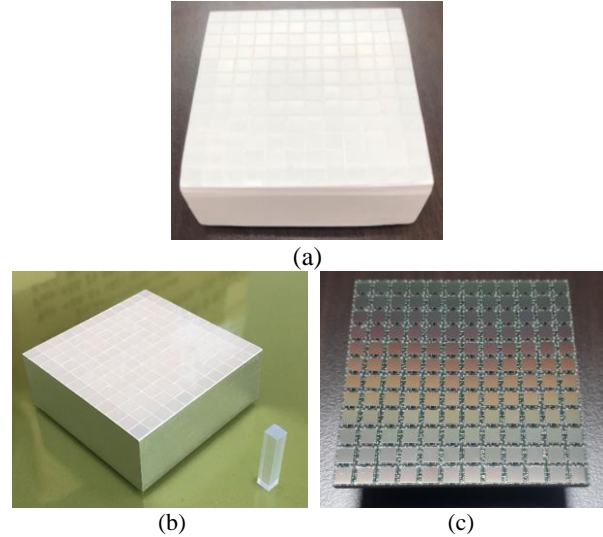


Fig. 1. Two pixelated stilbene scintillator (a), and plastic scintillator (EJ-276) array (b) with a size of $4 \times 4 \times 20 \text{ mm}^3$ and a pixel pitch of 4.2 mm. SiPM array (c) has the same number and area of pixels of these scintillator arrays.

2.1 Detector Configuration

Table 1. Comparison of the most prominent properties of plastic and stilbene scintillator.

	Plastic scintillator (EJ-276)	Stilbene
Density (g/cm^3)	1.096	1.15
Peak Emission (nm)	425	390
Decay Time (ns)	γ (13, 35, 270) n (13, 59, 460)	3.5 ~ 4.5
Light Yield (photons/MeV)	8,600	γ (14,000) n (10,700)
No. of H atoms / No. of C atoms	0.927	0.858

For PSD characteristics comparison experiments, the system was configured as follows to obtain signals from a detector that combines an EJ-276 scintillator array of 12×12 pixels coupled with SiPM array, as shown in Fig. 1. Plastic scintillator array (EJ-276) shows similar characteristics with Stilbene in terms of wavelength of maximum emission (425 nm), and density ($1.096 \text{ g}/\text{cm}^3$). However, it shows longer decay time (13, 35, 270 ns for gamma and 13, 59, 460 ns for neutron), smaller light

yield (8,600 photons/MeV), and higher ratio of number of H atoms to C atoms (0.927) as shown in Table 1. Due to these differences in characteristics, we would like to compare and analyze the effects on PSD separating neutrons and gamma. We are also looking for the smallest possible bias voltage that guarantees enough internal gain to separate signal due to photoelectron from noise.

2.2 Front-end readout circuit

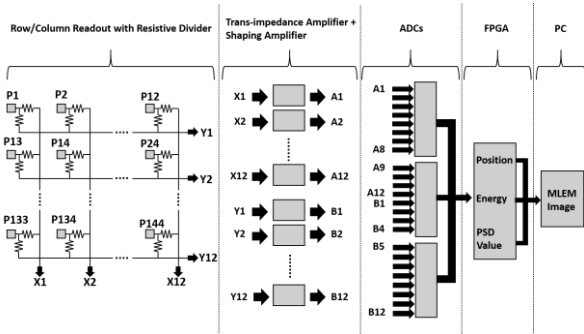


Fig. 2. Diagram for different types of front-end readout method adapting with and without filtering at shaping amplifier.

The front-end readout circuit used is prepared as shown in Fig. 2. Twenty-two transimpedance amplifiers (LMH6723, Texas Instruments) as pre-amplifiers for SiPM array were used for both X- and Y-axis for signal processing at each pixel at the front-end readout circuits. Filtering with a shaping amplifier softens the noise of the high-frequency components to obtain accurate energy, which is used as an important factor in pixel positioning. The amplified analog signals were digitized by three low-sampling rate ADCs (50 MHz, 8 channel, 12-bit, ADS5281, Texas Instruments). The field programmable gate arrays (FPGA) samples the digitized signals arriving at the ADC input and compares the discrete digital value with the trigger level set in the FPGA. If the new ADC value exceeds the trigger level, its value is stored in a buffer and transmitted to the internal computer that is used for running the MLEM algorithm from which the source image is reconstructed. The image data is then transferred via Wi-Fi or transmission control protocol/internet protocol (TCP/IP) to a remote side PC such as a desktop or laptop.

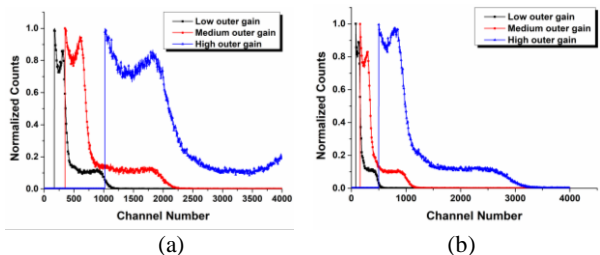


Fig. 3. Energy spectrum of pixelated stilbene scintillator (a), and plastic (b) measured for a ^{22}Na source as the bias voltage is fixed at 28 V but outer gain increased.

If the transimpedance amplifiers are employed, the feedback resistance must be large enough to obtain high outer gain and there is a trade-off between achieving high dynamic range and achieving low input-referred current noise for PSD capabilities. Fig.3 represents energy spectrums by measuring a ^{22}Na check source at 10 cm distance using three different outer gain when stilbene and plastic array mounted on SiPM, respectively. High gain is not able to compromise between the minimum and maximum of the desired dynamic range since it will be soon saturated, as shown in Fig.3(a). Because plastic scintillator has a low light yield when compared to stilbene, no saturation was observed in Fig.3(b).

2.3 Energy Calibration

Energy deposited by incident particles and corresponding light output in the plastic scintillator array is necessary for implementing low-energy light output detection thresholds and relating it back to its gamma-equivalent energy. The plastic scintillator is a low Z and low density material, and consequently its stopping power is rarely sufficient to capture the full energy of an incident γ ray. The absence of an observed photopeak necessitates that the energy calibration is performed on the Compton edges of clearly separated gamma-rays. Thus, ^{137}Cs and ^{22}Na gamma ray sources are used for the photon energy calibration as shown in Fig. 4. It is reckoned that this energy linearity of the detector module can be achieved by gain calibration for every pixel of the SiPM [8] because all pixel elements in the stilbene (or plastic) scintillator and SiPM array have slightly different light yield and gain factors, respectively.

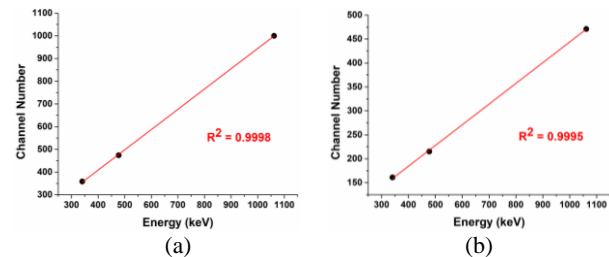


Fig. 4. The linear calibration curve for converting Compton edge height to light output measured for ^{137}Cs and ^{22}Na sources when the stilbene (a) and plastic array (b) mounted on SiPM operated with 28 V of bias voltage at 28°C. The Compton edge height was calculated at 70% at Compton peak from gamma-ray sources.

2.4 PSD method

PSD based on charge integration is implemented to exploit the characteristic difference observed in the tail-region of the measured pulses. The ratio of tail-integral to the peak provides a discriminating parameter that separates neutron and photon pulses. Figure 5 shows the

histogram distribution of the tail-to-peak ratio that yields two normally-distributed data corresponding to the neutron and photon detection.

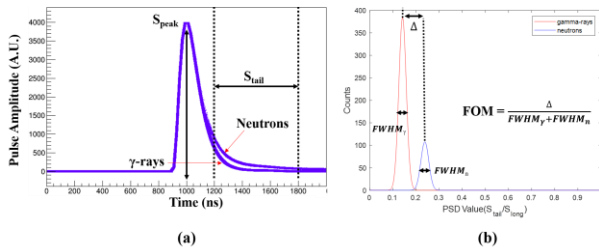


Fig. 5. Histogram of the tail-to-peak ratio showing the neutron and photon data distributions when exposed to a 3.5×10^5 n/s ^{252}Cf spontaneous fission source.

2.5 Figure-of-Merit (FoM) results

In addition to the PSD plot, figure of merit (FOM) values and profiles of neutron/gamma-ray separation at different energy regions (300 ± 100 keVee, 500 ± 100 keVee, 700 ± 100 keVee) are presented in Fig. 6. Stilbene-SiPM array module and plastic module were exposed to a 3.5×10^5 n/s ^{252}Cf spontaneous fission source for 2 hours. Both systems have a medium outer gain and operated with 28 V of bias voltage at 28°C . A clear distinction between neutron and gamma-ray events over the energy range of 200 keVee or more is observed by using the stilbene-SiPM array module, as shown in Fig. 6(a-b). On the other hand, Fig. 6(c-d) represents that the plastic array module shows an inferior PSD performance and we observed the distinction over the energy range of 500 keVee. The low sampling rate ADCs connected to the stilbene-SiPM array module more are capable of performing satisfactory PSD because the intrinsic particle separation of stilbene scintillator is sufficient due to its higher light yield than that of plastic scintillator.

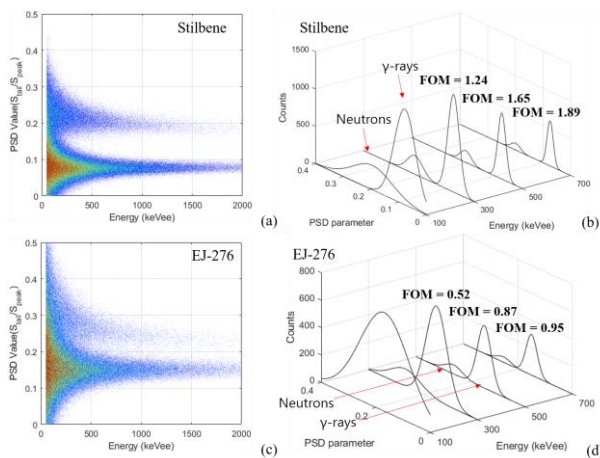


Fig. 6. PSD plot for 1,000,000 pulses measuring a 3.5×10^5 n/s ^{252}Cf spontaneous fission source for 2 hours with a threshold of 50 keVee (a, c), and distribution of PSD parameter at various energies (b, d) produced by the stilbene-SiPM module and plastic (EJ-276) module, in which both

systems have a medium outer gain and operated with 28 V of bias voltage.

3. Conclusions

The hand-held coded aperture based DPI system was realized by using the pixelated stilbene-SiPM array (12×12 pixels) module processed by multiplexed readout. The low sampling rate ADCs connected to the stilbene-SiPM array module are capable of performing satisfactory PSD over plastic-SiPM array module because stilbene has a higher light yield than that of plastic scintillator. We will present the comparison of PSD performance and reconstructed image quality produced by the DPI as using the two scintillator arrays.

Acknowledgements

This work was partly supported by Korea Institute of Energy Technology Evaluation and Planning (KETEP) grant funded by the Korea government (MOTIE) (20181520302230) and by the Nuclear Safety Research Program through the Korea Foundation of Nuclear Safety (KoFONS) using the financial resource granted by the Nuclear Safety and Security Commission (NSSC) of the Republic of Korea (No. 1903011-0119-CG100).

REFERENCES

- [1] Poitrasson-Rivière, Alexis, et al. Angular-resolution and material-characterization measurements for a dual-particle imaging system with mixed-oxide fuel. *Nucl. Instrum. Methods. Phys. Res. A.* 797, (2015) 278–284.
- [2] W. M. Steinberger, et. al. Imaging Special Nuclear Material Using a Handheld Dual Particle Imager. *Sci. rep.* 10(1), (2020) 1-11.
- [3] A. Poitrasson-Rivière, et al. Dual-particle imaging system based on simultaneous detection of photon and neutron collision events. *Nucl. Instrum. Methods. Phys. Res. A.* 760, (2014) 40–45.
- [4] H. Al Hamrashdi, D. Cheneler, and S. D. Monk, A fast and portable imager for neutron and gamma emitting radionuclides. *Nucl. Instrum. Methods. Phys. Res. A.* 953, (2020) 163253.
- [5] Kim, G. Digital n- γ pulse shape discrimination in organic scintillators with a high-speed digitizer. *J. Radiat. Prot. Res.* 44, (2019) 53-63.
- [6] M. J. Cieślak, K. A. Gamage, R. Glover, and C. J. Taylor, Pulse shape discrimination performance of a pixelated plastic scintillator (EJ-299-34) for a coded-aperture based dual particle imaging system. *J. Instrum.* 14, (2019) P07017.
- [7] G. Knoll, *Radiation Detection and Measurement.* (John Wiley & Sons, 2010). 581-582.
- [8] M. Jeong, B. Van, B. T. Wells, L. J. D’Aries, and M. D. Hammig, Scalable Gamma-ray Camera for Wide-Area Search Based on Silicon Photomultipliers Array. *Rev. Sci. Instrum.* 89 (2018) P033106.